

High thermoelectric performance of SnS under high pressure and high temperature

Yuqi Gao(高语崎), Xinglin Wang(王星淋), Cun You(由存), Dianzhen Wang(王殿振), Nan Gao(高楠), Qi Jia(贾琪), Zhihui Li(李志慧), Qiang Tao(陶强), and Pinwen Zhu(朱品文)

Citation: Chin. Phys. B, 2025, 34 (**8**): 087201. DOI: 10.1088/1674-1056/addbc8
http://cpb.iphy.ac.cn; http://iopscience.iop.org/cpb

What follows is a list of articles you may be interested in

High-entropy alloys in thermoelectric application: A selective review

Kai Ren(任凯), Wenyi Huo(霍文燚), Shuai Chen(陈帅), Yuan Cheng(程渊), Biao Wang(王彪), and Gang Zhang(张刚)

Chin. Phys. B, 2024, 33 (**5**): 057202. DOI: 10.1088/1674-1056/ad34c5

Ga intercalation in van der Waals layers for advancing p-type Bi_2Te_3-based thermoelectrics

Yiyuan Chen(陈艺源), Qing Shi(石青), Yan Zhong(钟艳), Ruiheng Li(李瑞恒), Liwei Lin(林黎蔚), Ding Ren(任丁), Bo Liu(刘波), and Ran Ang(昂然)

Chin. Phys. B, 2023, 32 (**6**): 067201. DOI: 10.1088/1674-1056/acc2af

Advancing thermoelectrics by suppressing deep-level defects in Pb-doped $AgCrSe_2$ alloys

Yadong Wang(王亚东), Fujie Zhang(张富界), Xuri Rao(饶旭日), Haoran Feng(冯皓然), Liwei Lin(林黎蔚), Ding Ren(任丁), Bo Liu(刘波), and Ran Ang(昂然)

Chin. Phys. B, 2023, 32 (**4**): 047202. DOI: 10.1088/1674-1056/acb765

Effect of carbon nanotubes addition on thermoelectric properties of $Ca_3Co_4O_9$ ceramics

Ya-Nan Li(李亚男), Ping Wu(吴平), Shi-Ping Zhang(张师平), Yi-Li Pei(裴艺丽), Jin-Guang Yang(杨金光), Sen Chen(陈森), and Li Wang(王立)

Chin. Phys. B, 2022, 31 (**4**): 047203. DOI: 10.1088/1674-1056/ac4bd2

Significant role of nanoscale Bi-rich phase in optimizing thermoelectric performance of Mg_3Sb_2

Yang Wang(王杨), Xin Zhang(张忻), Yan-Qin Liu(刘燕琴), Jiu-Xing Zhang(张久兴), Ming Yue(岳明)

Chin. Phys. B, 2020, 29 (**6**): 067201. DOI: 10.1088/1674-1056/ab84cd

---

SPECIAL TOPIC — Structures and properties of materials under high pressure

High thermoelectric performance of SnS under high pressure and high temperature

Yuqi Gao(高语崎), Xinglin Wang(王星淋), Cun You(由存), Dianzhen Wang(王殿振), Nan Gao(高楠), Qi Jia(贾琪), Zhihui Li(李志慧), Qiang Tao(陶强)†, and Pinwen Zhu(朱品文)‡

Synergetic Extreme Condition High-Pressue Science Center, State Key Laboratory of High Pressure and Superhard Materials, College of Physics, Jilin University, Changchun 130012, *China*

(Received 10 March 2025; revised manuscript received 18 May 2025; accepted manuscript online 22 May 2025)

Tin sulfide (SnS) is a promising non-toxic thermoelectric (TE) material to replace SnSe (Se is toxic), due to its similar structure and low thermal conductivity (κ) comparable to SnSe. However, the poor electrical conductivity (σ) of SnS results in lower TE performance. In this work, high pressure was utilized to regulate the electronic structure, thereby mediating the conflict of electron and phonon transport to optimize the TE performance. *In situ* measurements of thermoelectric properties for SnS under high pressure and high temperature revealed that although the Seebeck coefficient (S) and κ slightly decrease with increasing pressure, the σ dramatically increases with increasing pressure, finally increasing the dimensionless figure of merit (ZT). The σ increases from 2135 S·m^{-1} to 83549 S·m^{-1} as the pressure increases from 1 GPa to 5 GPa at 325 K, representing an increase of an order of magnitude. The high σ of SnS leads to an increase in the PF to 1436 μW·m^{-1}·K^{-2} at 5 GPa and 652 K. The maximum ZT value of 0.77 at 5 GPa and 652 K was obtained, which is 4 times the maximum ZT under ambient pressure and is comparable to that of doped SnS. The increase in σ is due to the fact that pressure modulates the band structure of SnS by narrowing the band gap from 1.013 eV to 0.712 eV. This study presents a valuable guide for searching new high TE performance materials using high pressure.

Keywords: thermoelectric materials, high pressure and high temperature, *in situ* measurement, SnS

PACS: 72.20.–i, 66.70.–f, 02.30.Cj, 71.20.–b

DOI: 10.1088/1674-1056/addbc8 **CSTR:** 32038.14.CPB.addbc8

1. Introduction

Thermoelectric (TE) materials are a kind of green energy material that can facilitate the direct and reversible conversion between heat and electrical energy without mechanical transmission or chemical processes.[1–3] To achieve high TE conversion efficiency, improving the dimensionless figure of merit ZT is the key,[4]

$$ZT = \frac{S^2\sigma T}{\kappa}, \tag{1}$$

where S is the Seebeck coefficient, σ is the electrical conductivity, T is the absolute temperature, and κ is the total thermal conductivity. Thus, high-performance thermoelectric materials need a high power factor ($PF = S^2\sigma$) and low κ. In the past few decades, SnSe with a special layered structure has made great progress in TE performance. Its high ZT is due to its strong anharmonicity, multiple valence bands, and three-dimensional (3D) charge and two-dimensional (2D) phonon transport.[5,6] However, the toxicity of Se^{2-} limits its application over a wide temperature range. Much effort has been made to substitute SnSe; for instance, PbTe, which is also a group IV–VI compound, has a similarly complex energy band structure. Tan *et al.*[7] used SrTe doping of PbTe to significantly improve the thermoelectric properties by means of band structure engineering and defect engineering. Finally, Na-doped PbTe-8%SrTe achieved a maximum ZT of 1.6 at 873 K. GeTe not only has the same crystal structure as SnSe but also shares the same strong anharmonicity. Duan *et al.*[8] used alloying and band structure engineering to obtain a maximum ZT value of 2.35 at 773 K. However, they contain not only rare heavy elements but also suffer from the disadvantages of toxicity and high cost. Therefore, it is still crucial to further develop low-cost, environmentally friendly, wide-temperature-range, and highly efficient thermoelectric materials.

Among these TE materials, SnS is an analog compound of SnSe, which is also predicted to be an attractive thermoelectric candidate. Compared with SnSe, SnS has also begun to attract attention because it has the same crystal structure, similar band structure, and an ultra-low κ (below 1.0 W·m^{-1}·K^{-1} above 400 K),[9–11] as well as lower cost, environmental friendliness, and more abundant raw materials (Sn and S). Therefore, SnS is a promising candidate to substitute SnSe due to its environmentally friendly nature, low cost, and high potential performance, making it appealing for large-scale commercial applications.

Although SnS shows great potential as a TE material due

†Corresponding author. E-mail: qiangtao@jlu.edu.cn

‡Corresponding author. E-mail: zhupw@jlu.edu.cn

© 2025 Chinese Physical Society and IOP Publishing Ltd. All rights, including for text and data mining, AI training, and similar technologies, are reserved.

to its high S and low κ, its poor conductivity limits further optimization of TE performance.[12] By taking advantage of the unique layered structure and strong anisotropy of SnS, He *et al.*[13] successfully prepared p-type SnS single crystals with high carrier mobility, leading to a maximum $ZT > 1.0$ at 873 K and a high device $ZT > 0.57$ from 300 to 873 K. Subsequently, He *et al.*[14] based on hole-doping, modulated the electronic band structure by introducing Se in p-type SnS, achieving a synergistic optimization of carrier mobility and effective mass. Finally, a maximum figure of merit ZT of ~ 1.6 at 873 K and an average ZT of ~ 1.25 from 300 to 873 K in $SnS_{0.91}Se_{0.09}$ crystals were obtained. However, the SnS single crystal's complex preparation process, stringent growth conditions, and poor mechanical properties (due to its layered structure) pose significant challenges for fabricating and developing thermoelectric devices based on p-type SnS single crystals. SnS polycrystalline materials can effectively solve this problem. Because SnS belongs to wide bandgap TE materials with a bandgap of 1.013 eV, the intrinsic electronic structure results in undoped SnS exhibiting extremely low σ (below 1 $S{\cdot}m^{-1}$ at 323 K) and low TE performance, with a ZT value of 0.16 at 823 K.[11] The optimization of the thermoelectric properties of polycrystalline SnS mainly involves carrier concentration optimization, band structure engineering, defect engineering, and so on.[15–18] For example, Yang *et al.*[15] successfully increased the hole carrier concentration in SnS by adjusting the molar ratio of the raw materials and introducing cationic vacancies, and obtained a maximum figure of merit ZT of ~ 0.8 at 873 K. Besides, Wu *et al.*[19] found that solid solution Se can not only change the band structure near the top of the valence band, reduce the average effective mass of the energy bands, strengthen the anisotropy of the Fermi surface, and improve the electrical transport properties, but also diminish the lattice thermal conductivity of p-type SnS polycrystals to ~ 0.3 $W{\cdot}m^{-1}{\cdot}K^{-1}$ at 820 K. Based on solid solution Se, the highest ZT value of ~ 1.1 at 820 K was obtained for $Na_{0.02}Sn_{0.98}S_{0.5}Se_{0.5}$ by optimizing the carrier concentration through Na doping. One of the effective strategies to improve its TE performance is doping with elements, which can optimize the carrier concentration (n) of SnS.[20–22] For example, Tan *et al.*[21] modulated n to 10^{18} cm^{-3} by Ag doping, thereby increasing it by three orders of magnitude, and a maximum ZT value of 0.6 was achieved at 923 K. P-type SnS polycrystalline materials doped with alkali metals (Li and Na) have been continuously developed; the maximum ZT values of Li- and Na-doped SnS were 0.66 at 848 K and 0.65 at 850 K, respectively.[20,22] However, the maximum ZT value of doped SnS remains below 0.7, which is a limitation. Breaking through this limitation is both challenging and significant for fabricating high-performance SnS-based TE materials. Many researchers have demonstrated that high pressure can significantly modulate the TE properties of materials without introducing other impurities.[23–30] The TE properties of materials are very sensitive to the electronic structure and lattice vibrations, which can be verified by applying pressure to compress the crystal structure. This is particularly effective for modulating the electronic structure by reducing the bandgap under high pressure. It can improve σ, leading to a higher PF. For example, Chen *et al.*[31] found that the σ of Cr-doped PbS can be significantly improved due to a pressure-driven topological phase transition, resulting in a high ZT value of 1.7 at room temperature. In addition, especially for layered materials, the effect is more pronounced. For example, in the layered thermoelectric material MoS_2, high-pressure induced stacking faults (SFs) enhance the interlayer interaction, resulting in a substantial increase in σ and a maximum ZT value of 0.191.[32] Combined with the inherently ultra-low κ of SnS, the optimization of electrical properties under high pressure may significantly enhance the TE performance of SnS. Therefore, uncovering TE transport behaviors under high pressure is crucial.

In this work, the TE performance of SnS was investigated through *in situ* measurements of TE transport properties under high pressure and high temperature (HPHT). The evolution of S and σ under HPHT was examined. Additionally, the κ and ZT under HPHT were estimated. The pressure-induced optimization of the band structure was analyzed. It was ultimately revealed that pressure can dramatically regulate the electronic structure to enhance the TE performance of SnS. This work provides a new perspective for the development of high-performance green TE materials.

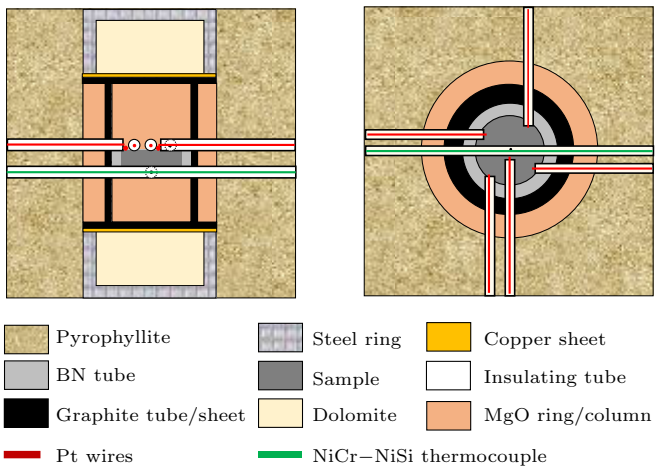


Fig. 1. Schematic diagram of *in situ* TE transport measurements under HPHT.

2. Method

2.1. Sample preparation and characterization

The polycrystalline SnS powder was purchased from Energy Chemical with a purity of 99.9%. Before the *in situ* measurements of thermoelectric properties under high pressure and high temperature, to accurately study the TE properties at HPHT, the powder sample was sintered by spark plasma

sintering (SPS) for 10 minutes at 873 K under 50 MPa in a vacuum atmosphere with a heating rate of 60 K per minute using the YLJ-SPS-T20 equipment. After the heat preservation step was completed, the sample was cooled down together with the furnace and the pressure was released. After sintering, cylindrical samples with a diameter of 6 mm and a thickness of 1.2 mm were obtained. The crystal phase composition of SnS was characterized by x-ray diffraction (XRD) (Rigaku D/Max 2550 V/PC, Japan, Cu $K\alpha$ radiation, $\lambda = 0.15418$ nm).

2.2. *In situ* measurement

After SPS treatment, a polished SnS wafer with a height of 1.0 mm and a diameter of 6.0 mm was loaded into the high-pressure assembly for *in situ* TE transport property measurements under HPHT using a 6×14400 kN cubic anvil apparatus, as shown in Fig. 1. The resistivity of SnS under HPHT was measured by the van der Pauw method. The relationship between sample resistivity ρ, sample thickness d, and relative resistances (R_A and R_B) is as[33]

$$\exp\left(-\frac{\pi d R_A}{\rho}\right) + \exp\left(-\frac{\pi d R_B}{\rho}\right) = 1, \tag{2}$$

where d was obtained from the Birch–Murnaghan equation of state,[34] $R_A = \frac{U_{cd}}{I_{ab}}$. $R_B = \frac{U_{bd}}{I_{ac}}$ (the subscript xy indicates that the current/voltage is across xy, where I is current and U is voltage). The Seebeck coefficient S was calculated from the temperature difference (ΔT) and voltage difference (ΔV) as

$$S = -\frac{\Delta V}{\Delta T}. \tag{3}$$

All test electrodes were platinum wires (0.2 mm in diameter), and temperature was measured using NiCr–NiSi thermocouples. A DC power supply and a Keithley multimeter (DMM6500) were used to generate DC current and measure the voltage drop, respectively. To ensure thermal equilibrium, after the temperature and pressure reached their set values, the system was left for 5 minutes before starting the data acquisition. More experimental details have been reported in previous studies.[35,36] SnS usually exhibits a *Pnma* phase crystal structure at room temperature and undergoes a reversible transformation to a more symmetric orthorhombic *Cmcm* phase at around 878 K.[37] To ensure that the thermoelectric properties of the high-temperature phase of SnS can be measured and remain stable, the testing temperature range was 321–968 K, and the common testing pressure range was 1–5 GPa.

2.3. Theoretical calculations

The Vienna *ab initio* simulation package (VASP) was used for spin-polarized density functional theory (DFT) calculations within the generalized gradient approximation (GGA) using the Perdew–Burke–Ernzerhof (PBE) functional formulation.[38–40] Projector augmented-wave (PAW) pseudopotentials were employed to describe the interactions between ionic cores and valence electrons. The valence electronic states were expanded in plane-wave basis sets with a cutoff energy of 500 eV. The DFT-D3 method was used to describe dispersion effects in the system. The electronic energy was considered self-consistent when the energy change was smaller than 10^{-5} eV, while a force convergence criterion of less than 0.02 eV/Å was used to determine the completion of geometry optimization. A k-point spacing of 0.03 Å^{-1} (corresponding to a k-point mesh of $3 \times 9 \times 9$) was used for geometry optimization.

3. Results and discussion

Figure 2(a) shows the crystal structure of SnS with lower symmetry, which features a special layered structure along the a-axis. The differences in atomic arrangement and bonding modes of the layered structure of SnS in different crystallographic directions lead to high anharmonicity, resulting in intrinsically low thermal conductivity.[41,42] As shown in Fig. 2(b), phase analysis by XRD indicates that the sample after *in situ* TE performance measurement has the crystal structure of the *Pnma* phase, consistent with the standard spectrum (PDF#39-354). Moreover, from the energy dispersive spectroscopy (EDS) mapping in Fig. S1, it can be seen that no loss of S or Sn elements occurred during SPS sintering and *in situ* HPHT thermoelectric property measurements. This is likely because both the SPS and HPHT methods achieve sealing of the samples under high pressure, resulting in no significant loss of elements. The SEM image of the SnS sample before the *in situ* HPHT measurement in Fig. 2(d) suggests that its grain shape is irregular lamellar, which is consistent with the crystal structure of SnS. As shown in Fig. 2(e), grains were broken after the *in situ* HPHT thermoelectric property measurement. Grain fragmentation resulted in smaller grain sizes, but the grain size remains at the micrometer level. Therefore, the increased grain boundary density has a very limited effect on reducing thermal conductivity.

The *in situ* TE transport properties of SnS under HPHT were investigated. Figures 3(a)–3(c) show the temperature-dependent TE transport properties of SnS under different high pressures. Figure 3(a) shows the temperature dependence of SnS σ under 1–5 GPa. The σ increases from 2135 S·m^{-1} to 83549 S·m^{-1} as the pressure increases from 1 GPa to 5 GPa at 325 K, representing an increase of an order of magnitude. For SnS crystals under high pressure, σ increases significantly with increasing pressure, reaching values two orders of magnitude higher than at ambient pressure. This significant increase in σ is attributed to high pressure effectively modulating the electronic structure, resulting in a reduced bandgap. The band structure usually has a strong response to pressure, especially in layered materials. Figures 3(d)–3(i) show the change of the band gap of SnS from ambient pressure to 5 GPa calculated by DFT calculations (GGA-PBE). The results show that the bandgap of SnS decreases from 1.013 eV to 0.712 eV with

increasing pressure. According to $K \cdot P$ theory,[43] the reduction of the bandgap leads to a reduction of carrier effective mass,[44] which in turn contributes to the improvement of carrier mobility. Meanwhile, according to the formula for carrier concentration

$$n = (N_c N_v)^{\frac{1}{2}} \exp\left(-\frac{E_g}{k_B T}\right). \tag{4}$$

The pressure-reduced bandgap favors an increase in carrier concentration. Therefore, the significant increase in σ is associated with the combined effect of the reduction in effective mass and the reduction in bandgap. At all pressures, the σ of SnS samples initially decreases and then increases with increasing temperature. In general, phonon scattering is the main scattering mechanism in semiconductors, which results in the decrease of mobility with increasing temperature. Therefore, at lower temperatures the conductivity decreases with increasing temperature, mainly due to the dominant role of carrier mobility in the conductivity. At higher temperatures, the conductivity increases with increasing temperature, mainly due to the increase of carrier concentration caused by thermal excitation.

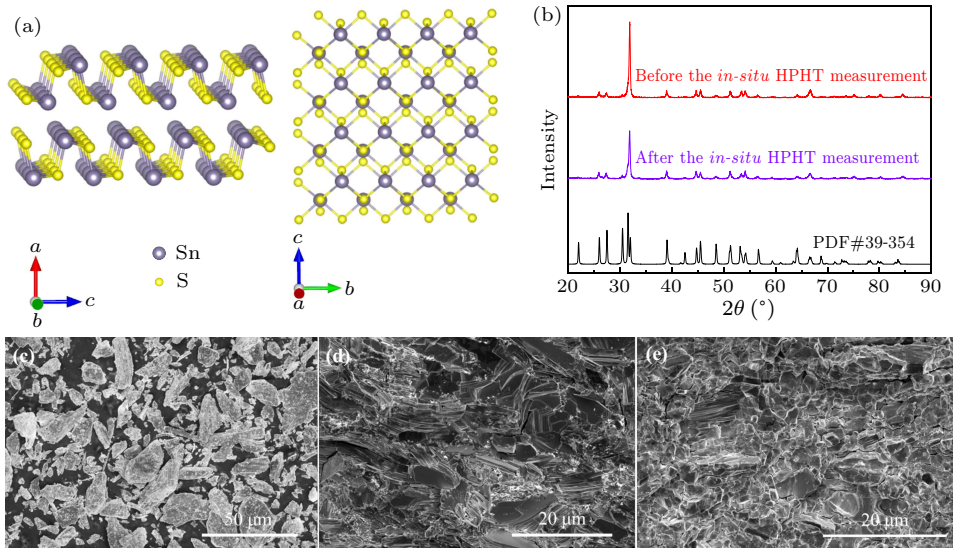


Fig. 2. (a) Crystal structure of SnS. (b) XRD patterns of SnS before and after the *in situ* HPHT measurement. SEM images of SnS sample: (c) purchased powder, (d) before, and (e) after the *in situ* HPHT measurement.

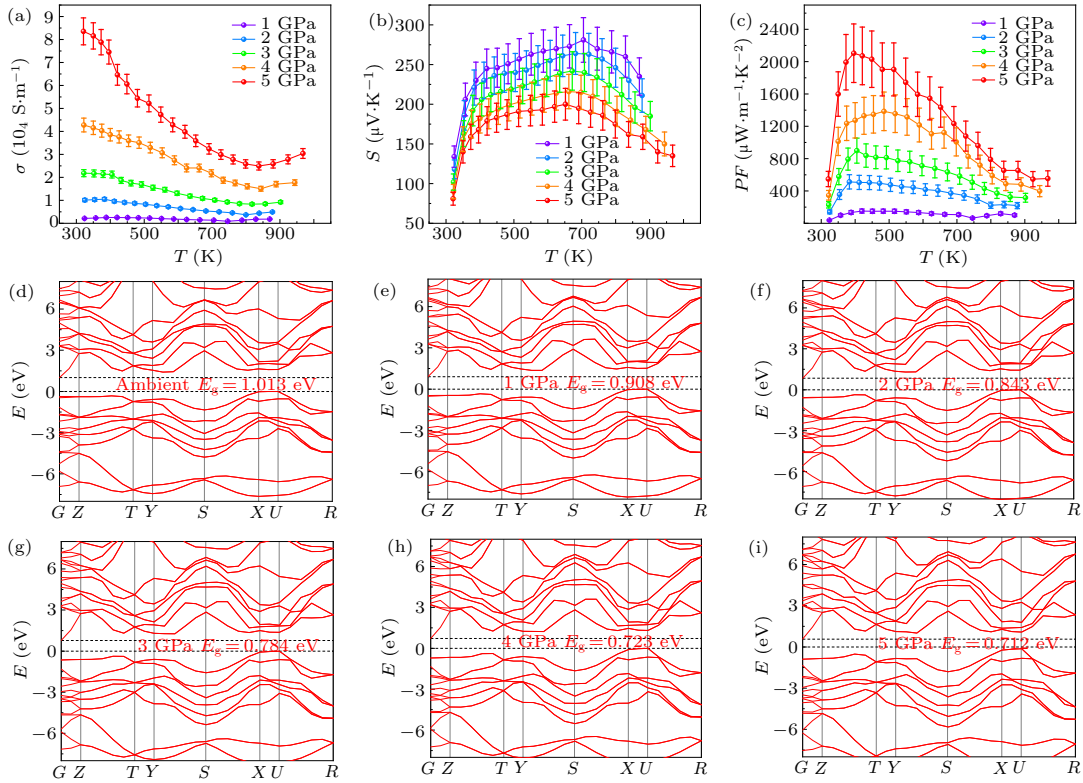


Fig. 3. Temperature-dependent (a) electrical conductivity, (b) Seebeck coefficient, and (c) power factor of SnS under different pressures. The dependence of E_g on pressure at (d) ambient pressure, (e) 1 GPa, (f) 2 GPa, (g) 3 GPa, (h) 4 GPa, and (i) 5 GPa.

Figure 3(b) shows the dependence of the Seebeck coefficient (S) of SnS on temperature under 1–5 GPa. The S remains positive, indicating that SnS is a p-type semiconductor. As pressure increases, S gradually decreases, showing the opposite trend to conductivity due to the interdependency of thermoelectric parameters. Under high pressure, the S of SnS samples follows a typical $\frac{3k_B}{2e}\ln T$ dependence as temperature increases. At low temperatures, few carriers are thermally excited. When the temperature exceeds about 700 K, S shows a significant drop caused by the onset of the bipolar effect resulting from thermal excitation. The bipolar effect is enhanced by the obvious narrowing of the bandgap under high pressure.[45,46] Therefore, increasing pressure intensifies the thermal excitation caused by temperature, leading to a decrease in the temperature at which S reaches its maximum value. As shown in Fig. 3(c), the PF of SnS increases with pressure. Although increasing pressure causes S to decrease slightly, the concurrent dramatic increase in σ more than compensates for this, resulting in a high PF of 1436 $\mu W\cdot m^{-1}\cdot K^{-2}$ at 5 GPa and 652 K.

Table 1. Comparison of electrical conductivity, Seebeck coefficient, and power factor extracted from previously reported SnS-based TE materials.

SnS-based TE materials	σ ($S\cdot m^{-1}$)	S ($\mu V\cdot K^{-1}$)	PF ($\mu W\cdot m^{-1}\cdot K^{-2}$)
Undoped $SnS_{823\ K}$ [13]	495	502.2	124.8
Ag-doped $SnS_{923\ K}$ [20]	2315	360	300
Na-doped $SnS_{850\ K}$ [21]	3266	313	320
Li-doped $SnS_{848\ K}$ [19]	1416	454	292
SnS at 5 $GPa_{652\ K}$ This work	35900	200	1436

As shown in Table 1, although the Seebeck coefficient (S) of SnS slightly decreases compared to that of doped SnS under ambient pressure, the σ is an order of magnitude higher. Consequently, a relatively high PF of 1436 $\mu W\cdot m^{-1}\cdot K^{-2}$ at 5 GPa and 652 K is obtained.

The κ of a semiconductor mainly consists of two parts: lattice thermal conductivity (κ_l) and carrier thermal conductivity (κ_e). Since the σ of SnS is extremely low under ambient pressure, the contribution of κ_e can be neglected. Therefore, under ambient pressure, κ_l is approximately equal to the total κ of SnS. The thermal conductivities of SnS under ambient pressure are shown in Fig. S2. The lattice thermal conductivity, κ_l, increases rapidly with increasing pressure. For pressures below 50 GPa, a linear model relating temperature and pressure can be expressed as[47]

$$\kappa_l(T,P) = \frac{a}{T}\left[\phi\left(1+\frac{B_0'}{B_0}P\right)^{\frac{1}{B_0'}} - \phi + 1\right], \tag{5}$$

where B_0 is the bulk modulus, B_0' is its pressure derivative, P is the pressure in GPa, a is a constant, and ϕ is a linear coefficient. For many materials measured experimentally under 5 GPa, $\phi \approx 7$,[47] which is adopted in this study. The values of B_0 and B_0' for SnS were obtained from Ehm *et al.*[48], with $B_0 = 36.6$ GPa and $B_0' = 5.5$ GPa. Furthermore, the term a/T corresponds to the temperature dependence of κ_l of SnS under ambient pressure. Thus, the variation of κ_l with temperature under high pressure can be obtained, as shown in Fig. 4(a). The lattice thermal conductivity values agree well with those predicted by Ouyang *et al.*[49] for SnS at various temperatures and pressures based on first-principles calculations. The increase of κ_l with pressure is attributed to the phonon hardening effect under high pressure.[50]

The carrier thermal conductivity, κ_e, of SnS under high pressure can be calculated using the Wiedemann–Franz law[51]

$$\kappa_e = L\sigma T, \tag{6}$$

where L is the Lorenz number, as shown in Fig. 4(b). An approximate method to estimate L is given by[52]

$$L = 1.5 + \exp\left(-\frac{|S|}{116}\right). \tag{7}$$

The total thermal conductivity, κ, is obtained by summing κ_e and κ_l, as shown in Fig. 4(c). The dramatic increase in electrical conductivity σ results in a considerable increase in κ_e, which further raises the total κ of SnS. However, due to the intrinsically low thermal conductivity of SnS, the overall κ remains relatively low. Finally, SnS exhibits a relatively low thermal conductivity of 1.21 $W\cdot m^{-1}\cdot K^{-1}$ at 5 GPa and 652 K.

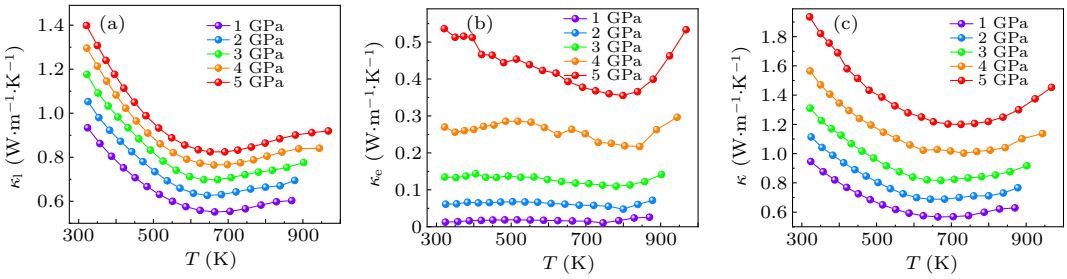


Fig. 4. Temperature dependence of (a) lattice thermal conductivity, (b) carrier thermal conductivity, and (c) total thermal conductivity.

Combined with the high power factor of SnS shown in Fig. 3(c), the ZT value has been significantly improved under HPHT. The ZT of SnS under HPHT is shown in Fig. 5(a). Owing to the substantial increase in electrical conductivity (σ) and the relatively low κ under HPHT, a maximum ZT value of 0.77 is obtained for SnS at 5 GPa and 652 K. It should be

noted that the optimal temperature range for TE performance in SnS decreases with increasing pressure. In other words, high pressure enables SnS to achieve higher TE performance over a wider temperature range. As shown in Fig. 5(b), the *ZT* value of SnS under HPHT is comparable to that of doped SnS at ambient pressure, demonstrating that high pressure has positively regulated the TE performance.

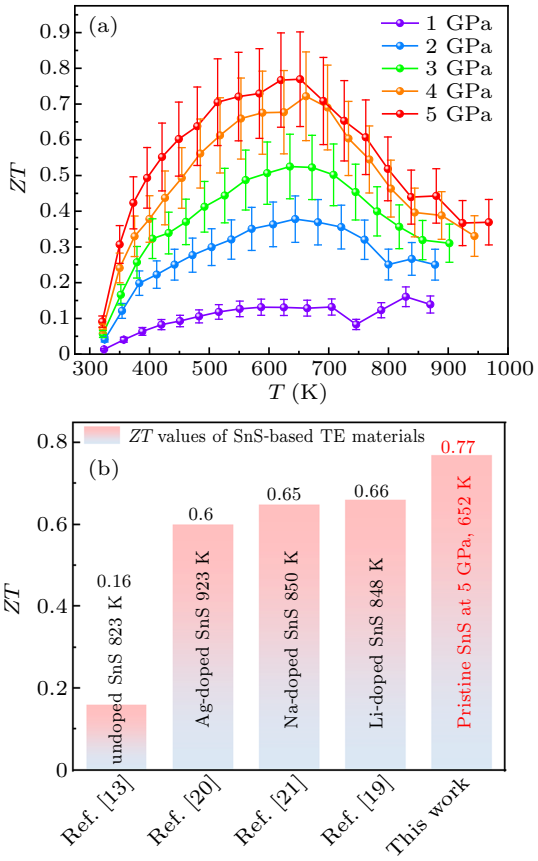


Fig. 5. (a) The *ZT* of SnS under different pressures; (b) Comparison of *ZT* values extracted from previously reported SnS-based TE materials.

4. Conclusion

In summary, the *in situ* measurements of thermoelectric properties for SnS under HPHT were investigated and analyzed. Although the Seebeck coefficient and thermal conductivity of SnS slightly decrease with increasing pressure, the σ dramatically increases to 35900 $S{\cdot}m^{-1}$ at 5 GPa and 652 K, which is two orders of magnitude higher than at ambient pressure, ultimately distinctly increasing the power factor to 1436 $\mu W{\cdot}m^{-1}{\cdot}K^{-2}$ at 5 GPa and 652 K. High pressure effectively modulates the electronic structure by narrowing the bandgap, which sharply improves the electrical conductivity of SnS. Finally, the optimum *ZT* value of SnS at 5 GPa and 652 K is 0.77, which is four times higher than the maximum *ZT* under ambient pressure and comparable to that of doped SnS. This study demonstrates that high pressure can effectively optimize wide-bandgap thermoelectric materials, which is significant for the search for new high-performance green TE materials.

Acknowledgements

The high-pressure experiments were performed at the B1 station of the Synergetic Extreme Condition User Facility (SECUF). The authors acknowledge funding support from the Program for the Development of Science and Technology of Jilin Province (Grant No. SKL202402004), the Jilin Province Major Science and Technology Program (Grant No. 20240211002GX), and the Open Research Fund of the Key Laboratory of Functional Materials Physics and Chemistry of the Ministry of Education (Jilin Normal University, 202405).

References

[1] Jiang B B, Yu Y, Cui J, Liu X X, Xie L, Liao J C, Zhang Q H, Huang Y, Ning S C, Jia B H, Zhu B, Bai S Q, Chen L D, Pennycook S J and He J Q 2021 *Science* **371** 830
[2] Jiang B B, Qiu P F, Chen H Y, Zhang Q H, Zhao K P, Ren D D, Shi X and Chen L D 2017 *Chem. Commun.* **53** 11658
[3] Shi X L, Zou J and Chen Z G 2020 *Chem. Rev.* **120** 7399
[4] Tan G J, Zhao L D and Kanatzidis M G 2016 *Chem. Rev.* **116** 12123
[5] Zhao L D, Lo S H, Zhang Y S, Sun H, Tan G J, Uher C, Wolverton C, Dravid V P and Kanatzidis M G 2014 *Nature* **508** 373
[6] Zhao L D, Tan G J, Hao S Q, He J Q, Pei Y L, Chi H, Wang H, Gong S K, Xu H B, Dravid V P, Uher C, Snyder G J, Wolverton C and Kanatzidis M G 2016 *Science* **351** 141
[7] Tan G J, Shi F Y, Hao S Q, Zhao L D, Chi H, Zhang X M, Uher C, Wolverton C, Dravid V P and Kanatzidis M G 2016 *Nat. Commun* **7** 12167
[8] Duan S C, Xue W H, Yao H H, Wang X Y, Wang C, Li S, Zhang Z W, Yin L, Bao X, Huang L H, Wang X D, Chen C, Sui J H, Chen Y, Mao J, Cao F, Wang Y M and Zhang Q 2022 *Adv. Energy Mater* **12** 2103385
[9] Parker D and Singh D J 2010 *J. Appl. Phys.* **108** 083712
[10] He W K, Wang D Y, Dong J F, Qiu Y, Fu L W, Feng Y, Hao Y J, Wang G T, Wang J F, Liu C, Li J F, He J Q and Zhao L D 2018 *J. Mater. Chem. A* **6** 10048
[11] Tan Q and Li J F 2014 *J. Electron. Mater.* **43** 2435
[12] Ge Z H, Zhao L D, Wu D, Liu X Y, Zhang B P, Li J F and He J Q 2016 *Mater. Today* **19** 227
[13] He W, Wang D Y, Dong J F, Qiu Y, Fu L W, Feng Y, Hao Y J, Wang G T, Wang J F, Liu C, Li J F, He J Q and Zhao L D 2018 *J. Mater Chem A* **6** 10048
[14] He W, Wang D Y, Wu H J, Xiao Y, Zhang Y, He D S, Feng Y, Hao Y J, Dong J F, Chetty R J, Hao L, Chen D F, Qin J F, Yang Q, Li X, Song J M, Zhu Y C, Xu W, Niu C L, Li X, Wang G T, Liu C, Ohta M, Pennycook S J, He J, Li J F and Zhao L D 2019 *Science* **365** 1418
[15] Yang H Q, Wang X Y, Wu H, Zhang B, Xie D D, Chen Y J, Lu X, Han X D, Miao L and Zhou X Y 2019 *J. Mater. Chem. C* **7** 3351
[16] Xue W H, Mao J, Liu K J, Zhang Q and Li J F 2024 *ACS Appl. Mater. Interfaces* **16** 38073
[17] Wu H, Peng K, Zhang B, Gong X N, Feng Z Z, Zhang X M, Xi M, Yan X M, Zhang Y S, Wang G Y, Lu X and Zhou X Y 2020 *Mater. Today Phys.* **14** 100221
[18] Asfandiyar, Cai B W, Zhao L D and Li J F 2020 *J. Materiomics* **6** 77
[19] Wu H, Peng K, Zhang B, Gong X N, Feng Z Z, Zhang X M, Xi M, Yan X M, Zhang Y S, Wang G Y, Lu X and Zhou X Y 2020 *Mater. Today Phys.* **14** 100221
[20] Niu Y, Chen Y D, Jiang J, Pan Y, Yang C C and Wang C 2020 *IOP Conf. Ser.: Mater. Sci. Eng.* **738** 012016
[21] Tan Q, Zhao L D, Li J F, Wu C F, Wei T R, Xing Z B and Kanatzidis M G 2014 *J Mater Chem A* **2** 17302
[22] Zhou B Q, Li S, Li W, Li J, Zhang X Y, Lin S Q, Chen Z W and Pei Y Z 2017 *ACS Appl. Mater. Interfaces* **9** 34033
[23] Ovsyannikov S V, Shchennikov V V, Vorontsov G V, Manakov A Y, Likhacheva A Y and Kulbachinski V A 2008 *J. Appl. Phys.* **104** 053713

[24] Ovsyannikov S V, Shchennikov V V, Manakov A Y, Likhacheva A Y, Ponosov Y S, Mogilenskikh V E, Vokhmyanin A P, Ancharov A I and Skipetrov E P 2009 *Phys. Status Solidi B* **246** 615

[25] Ovsyannikov S V, Shchennikov V V, Ponosov Y S, Gudina S V, Guk V G, Skipetrov E P and Mogilenskikh V E 2004 *J. Phys. D: Appl. Phys.* **37** 1151

[26] Ovsyannikov S V and Shchennikov V V 2007 *Appl. Phys. Lett.* **90** 122103

[27] Ovsyannikov S V and Shchennikov V V 2004 *Physica B* **344** 190

[28] Zhao D Y, Yang M M, Sun H R, Chen X, Zhang Y S and Liu X B 2023 *Chin. Phys. B* **32** 107305

[29] Zheng B W, Chen T, Sun H R, Yang M M, Yang B C, Chen X, Zhang Y S and Liu X B 2024 *Chin. Phys. Lett.* **41** 057301

[30] Han S, Duan S, Liu Y X, Wang C, Chen X, Sun H R and Liu X B 2023 *Chin. Phys. B* **32** 016101

[31] Chen L C, Chen P Q, Li W J, Zhang Q, Struzhkin V V, Goncharov A F, Ren Z F and Chen X J 2019 *Nat. Mater.* **18** 1321

[32] Wang D Z, Zou J, You C, Ge Y F, Wang X L, Liang X, Zhou Q, Tao Q, Chen Y L, Zhu P and Cui T 2024 *Appl. Phys. Lett.* **125** 213903

[33] Matsumura T and Sato Y 2010 *Journal of Modern Physics* **01** 340

[34] Birch F 1938 *J. Appl. Phys.* **9** 279

[35] Zhao W, Cheng J E, Wang D Z, You C, Zhang J M, Ye M Y, Wang X, Dong S S, Tao Q and Zhu P W 2022 *Rev. Sci. Instrum.* **93** 103901

[36] Zhao W, Cheng J E, Li Y, Ye M Y, Wang D Z, Wang L, Gai X M, You C, Qu X, Tao Q and Zhu P W 2023 *Appl. Phys. Lett.* **123** 062202

[37] Norton K J, Alam F and Lewis D J 2021 *Appl. Sci-Basel* **11** 2062

[38] Li F, Tian Y H, Su S B, Wang C S, Li D S, Cai D D and Zhang S Q 2021 *Appl. Catal. B* **299** 120665

[39] Tang M and Ge Q F 2017 *Chin. J. Catal.* **38** 1621

[40] Hafner J 2008 *J. Comput. Chem.* **29** 2044

[41] Rundle J and Leoni S 2022 *J. Phys. Chem. C* **126** 14036

[42] Li W T and Yang C X 2023 *Physica E* **145** 115521

[43] Bastos C M O, Sabino F P, Junior P E F, Campos T, Silva J L F D and Sipahi G M 2016 *Semicond. Sci. Technol.* **31** 105002

[44] Errandonea D, Sanchez-Royo J F, Segura A, Chevy A and Roa L 1998 *High Pressure Res.* **16** 13

[45] Guo Z, Song K, Yan Z P, Sun P, Tan X J, Wu G, Zhang Q, Liu G Q, Yu B and Jiang J 2021 *Chem. Eng. J.* **426** 131853

[46] Wang D Z, You C, Ge Y f, Wang F, Wang X L, Liang X, Zhou Q, Tao Q, Chen Y L and Zhu P W 2024 *Appl. Phys. Lett.* **125** 013903

[47] Manga M and Jeanloz R 1997 *J. Geophys. Res. Solid Earth* **102** 2999

[48] Ehm L, Knorr K, Dera P, Krimmel A, Bouvier P and Mezouar M 2004 *J. Phys.: Condens. Matter* **16** 3545

[49] Ouyang N, Wang C and Chen Y 2022 *Int. J. Heat Mass Transfer* **192** 122859

[50] Wu J, Zhang H, Wang T Y, Qian X, Song B, Liu T H and Yang R G 2023 *Int. J. Heat Mass Transfer* **208** 124092

[51] Borup K A, de Boor J, Wang H, Drymiotis F, Gascoin F, Shi X, Chen L, Fedorov M I, Mueller E, Iversena B B and Snyder G J 2015 *Energy Environ. Sci.* **8** 423

[52] Kim H S, Gibbs Z M, Tang Y, Wang H and Snyder G J 2015 *APL Mater.* **3** 041506